

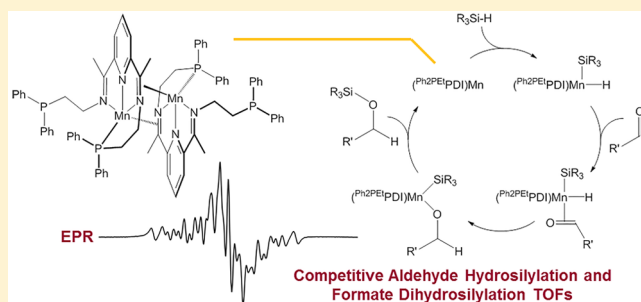
Hydrosilylation of Aldehydes and Formates Using a Dimeric Manganese Precatalyst

Tufan K. Mukhopadhyay, Chandrani Ghosh, Marco Flores, Thomas L. Groy, and Ryan J. Trovitch*

School of Molecular Sciences, Arizona State University, Tempe, Arizona 85287, United States

Supporting Information

ABSTRACT: The formally zero-valent Mn dimer $[(\text{Ph}_2\text{PEtPDI})\text{Mn}]_2$ has been synthesized upon reducing $(\text{Ph}_2\text{PEtPDI})\text{MnCl}_2$ with excess Na/Hg. Single crystal X-ray diffraction analysis has revealed that $[(\text{Ph}_2\text{PEtPDI})\text{Mn}]_2$ possesses a κ^4 -PDI chelate about each Mn center, as well as η^2 -imine coordination across the dimer. The chelate metrical parameters suggest single electron PDI reduction and EPR spectroscopic analysis afforded a signal consistent with two weakly interacting $S = 1/2$ Mn centers. At ambient temperature in the absence of solvent, $[(\text{Ph}_2\text{PEtPDI})\text{Mn}]_2$ has been found to catalyze the hydrosilylation of aldehydes at loadings as low as 0.005 mol % (0.01 mol % relative to Mn) with a maximum turnover frequency of $9,900 \text{ min}^{-1}$ ($4,950 \text{ min}^{-1}$ per Mn). Moreover, the $[(\text{Ph}_2\text{PEtPDI})\text{Mn}]_2$ -catalyzed dihydrosilylation of formates has been found to proceed with turnover frequencies of up to 330 min^{-1} (165 min^{-1} relative to Mn). These metrics are comparable to those described for the leading Mn catalyst for this transformation, the propylene-bridged variant $(\text{Ph}_2\text{PPrPDI})\text{Mn}$; however, $[(\text{Ph}_2\text{PEtPDI})\text{Mn}]_2$ is more easily inhibited by donor functionalities. Carbonyl and carboxylate hydrosilylation is believed to proceed through a modified Ojima mechanism following dimer dissociation.



INTRODUCTION

In laboratory and industrial settings, the reduction of carbonyl-containing compounds remains a popular synthetic route to organic alcohols.¹ This transformation can be achieved with inorganic hydride reagents² or under hydrogen in the presence of a catalyst;³ however, due to the flammable nature of these reductants, hydrosilylation has gained traction as a mild and operationally simple approach to C=O bond reduction.⁴ While precious metal catalysts are known to mediate this transformation,⁵ poor selectivity, toxicity, and metal cost have prompted the search for sustainable base metal alternatives. Despite the tendency of first-row metals to engage in one-electron chemistry,⁶ many efficient Fe,⁷ Co,⁸ Ni,⁹ Cu,¹⁰ and Zn¹¹ carbonyl hydrosilylation catalysts have been reported. The activities and lifetimes of these catalysts can rival their precious metal counterparts; however, additional improvement of carbonyl hydrosilylation turnover frequency (TOF) remains difficult to achieve.

To some extent, this challenge has been met through the development of Mn catalysts.^{12,13} In the 1990s, Cutler and co-workers reported that $(\text{Ph}_3\text{P})(\text{CO})_4\text{MnC}(\text{O})\text{Me}$ exhibits ketone hydrosilylation¹⁴ TOFs of up to 27 min^{-1} and ester reduction¹⁵ TOFs of up to 4 min^{-1} at ambient temperature. Several well-defined Mn catalysts for carbonyl hydrosilylation have since been described;^{16–20} however, higher activity has only been demonstrated in a few instances. In 2013, Chidara and Du reported that $(3,5\text{-}^t\text{Bu-salen})\text{MnN}$ hydrosilylates aldehydes with TOFs as high as 196 min^{-1} , but only when

the reaction is heated ($80 \text{ }^\circ\text{C}$).¹⁷ In 2014, we found that the propylene-bridged bis(imino)pyridine (or pyridine diimine, PDI) compound, $(\text{Ph}_2\text{PPrPDI})\text{Mn}$ (Figure 1, left), mediates

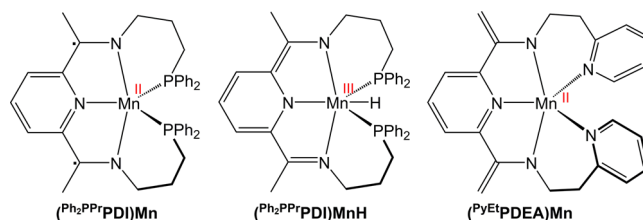


Figure 1. Manganese hydrosilylation catalysts featuring κ^5 -ligands.^{18–20}

ketone hydrosilylation with TOFs of up to $76\,800 \text{ h}^{-1}$ (more accurately expressed as 1280 min^{-1}) and the dihydrosilylation of esters (to yield silyl ethers) with modest TOFs of up to 18 h^{-1} at $25 \text{ }^\circ\text{C}$ in the absence of solvent.¹⁸ Under these conditions, we recently reported that $(\text{Ph}_2\text{PPrPDI})\text{Mn}$ catalyzes aldehyde hydrosilylation with TOFs of 4900 min^{-1} and formate dihydrosilylation with TOFs of 330 min^{-1} .¹⁹ Importantly, $(\text{Ph}_2\text{PPrPDI})\text{Mn}$ is believed to mediate carbonyl hydrosilylation through a modified Ojima mechanism while a related catalyst, $(\text{Ph}_2\text{PPrPDI})\text{MnH}$ (Figure 1, middle), achieves comparable

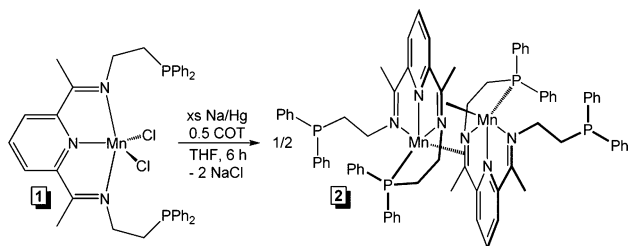
Received: June 7, 2017

formate hydrosilylation TOFs through a hydride insertion mechanism.¹⁹ Efforts to develop structurally related Mn catalysts have also led us to evaluate the hydrosilylation activity of ethylpyridine-substituted (^{PyEt}PDEA)Mn (Figure 1, right), which exhibits a lower maximum benzaldehyde hydrosilylation TOF of 2475 min⁻¹.²⁰ Herein, we describe our efforts to prepare and evaluate a Mn hydrosilylation precatalyst supported by ^{Ph₂PEt}PDI,²¹ which possesses an ethylene-bridge between the imine and phosphine donors.

RESULTS AND DISCUSSION

Heating a 1:1 mixture of ^{Ph₂PEt}PDI²¹ and (THF)₂MnCl₂ in toluene to 125 °C afforded a pale orange solid identified as (^{Ph₂PEt}PDI)MnCl₂ (**1**, Scheme 1). This compound was found to

Scheme 1. Preparation of [(^{Ph₂PEt}PDI)Mn]₂ (**2**)



be NMR silent and exhibit an ambient temperature magnetic susceptibility of 6.0 μ_B (magnetic susceptibility balance, 25 °C), consistent with a high-spin Mn(II) environment ($S_{Mn} = 5/2$). On the basis of these observations, and prior structural characterization of (^{Ph₂PPt}PDI)MnCl₂¹⁸ and (^{PyEt}PDI)MnCl₂,²⁰ it is reasonable to propose that **1** possesses a κ^3 -N,N,N-^{Ph₂PEt}PDI chelate. Reduction of **1** using excess Na/Hg in the presence of 1,3,5,7-cyclooctatetraene (added to facilitate reduction)^{18,20} afforded a red paramagnetic complex identified as [(^{Ph₂PEt}PDI)Mn]₂ (**2**, Scheme 1). The ¹H NMR spectrum of **2** features broadened resonances at 32.26 and 26.23 ppm (Figure S1). A single, broad resonance was also observed in the ³¹P NMR spectrum at -58.49 ppm (Figure S2, likely due to uncoordinated phosphine substituents) and the solution state magnetic moment of this compound was found to be 3.3 μ_B at 25 °C, suggesting two unpaired electrons in the ground state.

To obtain structural information, a single crystal of **2** was analyzed by X-ray diffraction. Refinement revealed a dimeric arrangement whereby each Mn center is supported by a κ^4 -PDI chelate (Figure 2). Each Mn center is also coordinated to the imine bond of a neighboring (PDI)Mn moiety in an η^2 -fashion [Mn(1)–C(8A) and Mn(1)–N(3A) are 2.233(6) and 1.977(4) Å, respectively]. This interaction results in C(8)–N(3) elongation to 1.395(6) Å, relative to the average uncoordinated PDI imine C=N distance of 1.271(17) Å,²² indicative of significant metal-to-ligand backbonding. The geometry about Mn is best described as distorted trigonal bipyramidal with N(1)–Mn(1)–N(3), N(2)–Mn(1)–P(1), and N(2)–Mn(1)–N(3A) angles of 150.85(16), 129.25(12), and 100.30(15)°, respectively. The unbridged portion of each PDI chelate features an elongated N(1)–C(2) distance of 1.338(6) Å and a contracted C(2)–C(3) distance of 1.425(7) Å. Although **2** is formally zero-valent, these distances are consistent with single electron α -diimine (DI) reduction,²³ whereby the PDI-based electron density resides on the unbridged backbone atoms. The Mn(1)–N(1), Mn(1)–

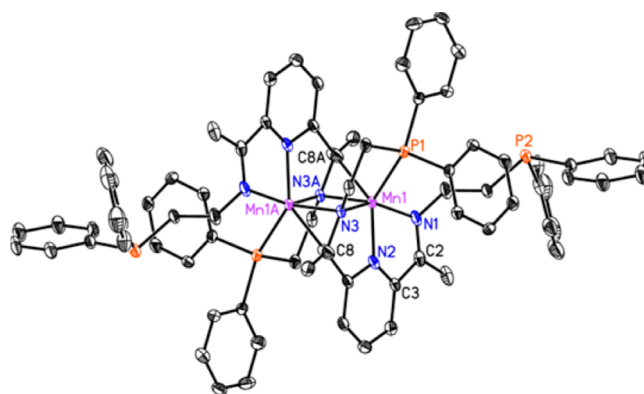


Figure 2. Molecular structure of **2** shown at 30% probability ellipsoids. Hydrogen atoms and cocrystallized toluene molecules (4 per dimer) are omitted for clarity. For complete list of metrical parameters, see Table S2.

N(2), and Mn(1)–N(3) distances were determined to be 2.022(4), 1.947(4), and 2.092(4) Å, respectively, and the two Mn centers are 2.7889(14) Å apart. Considering these metrical parameters and the observed magnetic moment, it can be proposed that **2** features intermediate spin Mn(I) centers that are antiferromagnetically coupled to their respective singly reduced supporting DI moieties.

To further investigate the electronic structure of **2**, a toluene solution of this complex was prepared and analyzed by X-band (9.40 GHz) EPR spectroscopy at 107 K (Figure 3). The

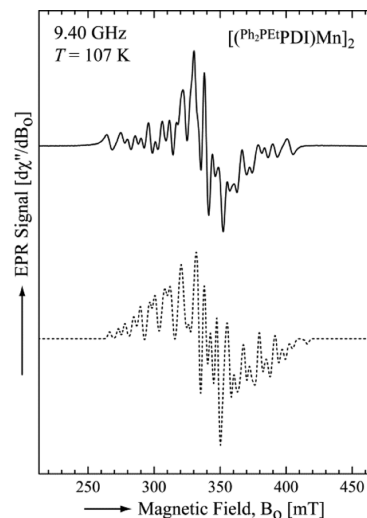


Figure 3. Experimental (solid line) and simulated (dashed line) X-band EPR spectra of **2** in toluene at 107 K. These spectra showed small discrepancies for the magnetic field resonances above 390 mT. Such discrepancies, as well as the differences in line intensities, might be due to inhomogeneities present in the frozen solution (powder) sample.

observed spectral features are consistent with the presence of two manganese centers, i.e., a broad signal showing a multilined pattern due to hyperfine coupling (hfc) interactions between the magnetic moment of an unpaired electron system and the magnetic moment of a neighboring ⁵⁵Mn ($I = 5/2$) nuclei. On the basis of the electronic structure model proposed above, each Mn center was assumed to carry one net unpaired electron that results in an electronic configuration with two unpaired

electrons present in **2**. Thus, the best fit of the EPR spectrum, corresponding to **2**, was obtained considering a triplet state ($S = 1$) as the ground state of the electron spin system (see the [Experimental Section](#) for the definition of the spin Hamiltonian). The parameters that were obtained from the fit are summarized in [Table 1](#). The g values are anisotropic and reflect

Table 1. Parameters Used to Fit the EPR Spectrum of **2** at 9.40 GHz and $T = 107$ K

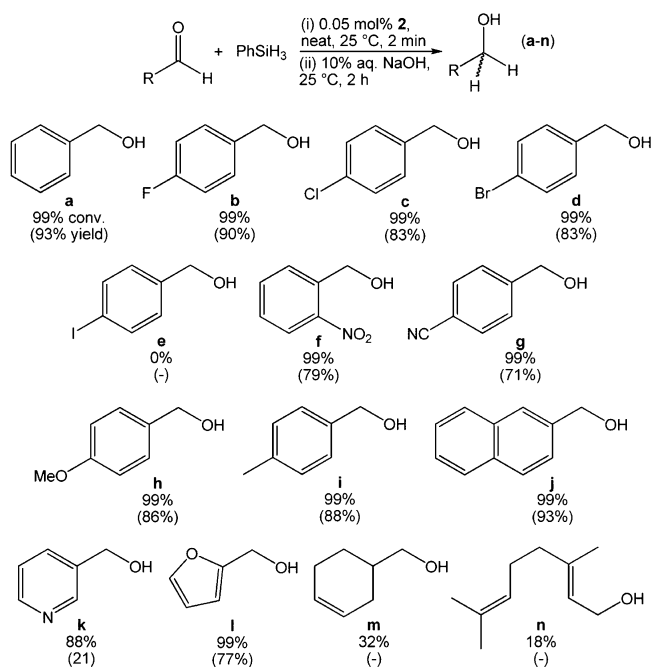
parameter ^a	2
g_x	2.037
g_y	1.980
g_z	1.893
$ D $	$77.7 \times 10^{-4} \text{ cm}^{-1}$
$ E $	$2.0 \times 10^{-4} \text{ cm}^{-1}$
$ A_x^{Mn} $	$114.1 \times 10^{-4} \text{ cm}^{-1}$
$ A_y^{Mn} $	$43.7 \times 10^{-4} \text{ cm}^{-1}$
$ A_z^{Mn} $	$94.7 \times 10^{-4} \text{ cm}^{-1}$

^aSee the [Experimental Section](#) for the definition of the fitting parameters.

a large electron spin delocalization which is consistent with the crystallographically determined molecular structure of **2**. The zero-field splitting (ZFS) parameters are relatively small and show a nearly axial ZFS (i.e., $D \ll g\beta_e B_0/h$, and $E/D \approx 0$). This finding indicates weak electron–electron repulsion between the two unpaired electrons present in **2**.

Compound **2** was then screened for carbonyl hydrosilylation activity. When a neat mixture of benzaldehyde and PhSiH_3 was added to 0.05 mol % **2** (0.1 mol % relative to Mn) at room temperature, an exothermic reaction ensued, resulting in complete conversion to a mixture of silyl ethers after 2 min. Hydrolysis with 10% aqueous NaOH solution followed by extraction afforded benzyl alcohol in 93% yield ([Table 2](#), entry a). Thirteen additional aldehydes were screened, and the reaction outcomes are summarized in [Table 2](#) (entries b–n).

Table 2. Hydrosilylation of Aldehydes Using **2**

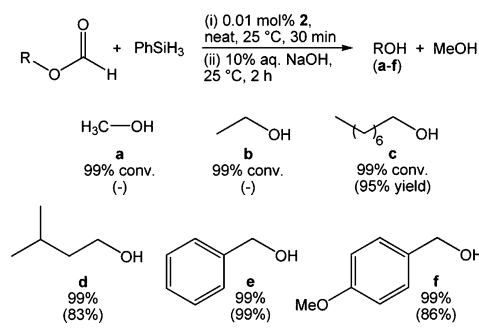


Precatalyst **2** has been found to tolerate fluoro, chloro, and bromo functionalities (entries b–d), but not the iodo functionality of 4-iodobenzaldehyde (entry e). This substrate did not participate in an exothermic reaction with PhSiH_3 and **2** due to catalyst decomposition. Complex **2** was tolerant of the nitro and nitrile groups of 2-nitrobenzaldehyde (entry f) and 4-cyanobenzaldehyde (entry g), respectively, as these functionalities were not reduced under the reaction conditions. Electron donating substituents on the aryl ring also do not influence efficiency, as seen in the case of *p*-anisaldehyde and *p*-tolualdehyde (entries h–i). Heteroaromatic aldehydes were hydrosilylated without difficulty (entries k–l), however, it should be noted that pyridine-3-carboxaldehyde did not reach complete conversion (88%) after 2 min. Moreover, the aldehyde functionality of 3-cyclohexene-1-carboxaldehyde (entry m) and citral (entry n) was not efficiently reduced during the 2 min time frame of the experiment. Under the same conditions, $(\text{Ph}^2\text{PPrPDI})\text{Mn}$ was found to fully reduce the aldehyde functionality of these substrates,¹⁹ suggesting that **2** is more susceptible to inhibition due to olefin coordination. Olefin hydrosilylation was not observed and attempts to hydrosilylate 1-hexene using **2** and PhSiH_3 were unsuccessful, even at 120 °C. The neat hydrosilylation of acetophenone and cyclohexanone using 0.05 mol % **2** (0.1 mol % relative to Mn) was also performed and both substrates were fully converted to a mixture of silyl ethers after 4 min (TOF = 495 and 248 min^{-1} relative to Mn). In general, we have found that it takes several seconds longer for neat hydrosilylation reactions featuring **2** to exotherm, relative to when $(\text{Ph}^2\text{PPrPDI})\text{Mn}$ is employed as the catalyst.

Efforts were also made to optimize **2**-mediated aldehyde hydrosilylation using a stoichiometric quantity of PhSiH_3 . Lowering the catalyst loading to 0.005 mol % (0.01 mol % relative to Mn) did not diminish benzaldehyde hydrosilylation conversion after 2 min under neat conditions, equating to a maximum TOF of 9,900 min^{-1} (4,950 min^{-1} per Mn). On the basis of per Mn turnover, this activity matches what was observed for $(\text{Ph}^2\text{PPrPDI})\text{Mn}$ -catalyzed benzaldehyde hydrosilylation;¹⁹ however, the same conversion rate could not be achieved using other substrates in [Table 2](#). For example, repeating this procedure with 4-fluorobenzaldehyde resulted in 18% conversion after 2 min, equating to a TOF of 1800 min^{-1} (900 min^{-1} per Mn).

Attempts to hydrosilylate benzaldehyde using AIBN (radical initiator), Mn powder, $(\text{THF})_2\text{MnCl}_2$, or $(\text{Ph}^2\text{PEtPDI})\text{MnCl}_2$ as the catalyst did not result in substrate conversion. Moreover, performing this reaction in the presence of excess Hg^0 did not adversely affect conversion, suggesting that **2** remains homogeneous throughout catalysis. Additionally, benzaldehyde hydrosilylation was not inhibited when the reaction was conducted in the dark, suggesting that phosphine dissociation via photolysis is not required for catalysis to occur. This contrasts recent work showing that CpMn carbonyl catalysts achieve Si–H oxidative addition following photolytic loss of two CO ligands.^{16e} Adding 2 equiv of NaEt_3BH to **1** did not allow for the observation or isolation of a catalytically relevant hydride complex.

Compound **2** was also employed as a formate dihydrosilylation precatalyst. When a neat equimolar mixture of methyl formate or ethyl formate and PhSiH_3 was added to 0.01 mol % **2** (0.02 mol % relative to Mn), an exothermic reaction was observed along with >99% conversion to silyl ethers within 30 min ([Table 3](#), entries a–b). Alkaline hydrolysis of the

Table 3. Dihydrosilylation of Formates Using **2**

corresponding products was performed; however, the low boiling points of MeOH and EtOH did not allow for their isolation through evaporation. Furthermore, the reaction scale was not large enough to separate these products by short path distillation. To address this issue, our investigation shifted to the dihydrosilylation of higher molecular weight formates. As shown in Table 3, **2** was found to catalyze the dihydrosilylation of octyl (entry c), isoamyl (entry d), benzyl (entry e), and *p*-anisyl formate (entry f) under the same conditions. Following workup with 10% aqueous NaOH, extraction with Et₂O, and removal of the solvent and generated MeOH, the corresponding alcohols were isolated in good yield. The observed **2**-mediated formate dihydrosilylation TOFs of 330 min⁻¹ (165 min⁻¹ relative to Mn) are slower than those observed for (Ph₂PPrPDI)Mn on a per Mn basis¹⁹ but greater than all other reported transition metal examples.²⁴ The dihydrosilylation of ethyl acetate using 1.0 mol % **2** and equimolar PhSiH₃ in benzene-*d*₆ was also performed and reduction to PhSi(OEt)₃ was observed after 7.2 h at 25 °C (TOF = 14 h⁻¹). This is again slower than the 5.5 h needed to complete ethyl acetate dihydrosilylation using (Ph₂PPrPDI)Mn.¹⁸

Considering our recent mechanistic investigation of (Ph₂PPrPDI)Mn-mediated hydrosilylation¹⁹ and the observations described herein, it is proposed that **2** mediates carbonyl hydrosilylation and carboxylate dihydrosilylation through a modified Ojima mechanism (Figure 4). Upon dissociating into monomeric (Ph₂PEtPDI)Mn, Si-H oxidative addition would afford the silyl hydride intermediate shown at the top right. Alternatively, unproductive donor association may occur at this point and inhibit hydrosilylation. Once silane activation takes place, substrate coordination and insertion into Mn-H would

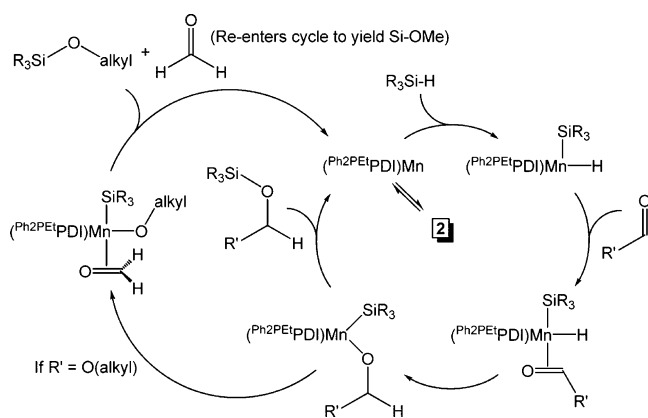


Figure 4. Modified Ojima mechanism proposed for **2**-mediated carbonyl and carboxylate hydrosilylation.

yield a silyl alkoxide intermediate that undergoes reductive elimination to afford the respective silyl ether. In the case of carboxylates, the silyl alkoxide intermediate is believed to undergo fast β -alkoxide elimination to yield the silyl ether product and an equivalent of formaldehyde, as described for (Ph₂PPrPDI)Mn.¹⁹ Formaldehyde is quickly hydrosilylated under the reaction conditions to yield methoxysilane equivalents. Given our observations of delayed catalytic onset and slower ethyl acetate dihydrosilylation, it is believed that dimer **2** acts as the catalyst resting state. Our inability to observe a Mn hydride complex upon adding of **2** equiv of NaEt₃BH to **1** also suggests that catalysis is unlikely to proceed through a straightforward insertion mechanism analogous to the one described for (Ph₂PPrPDI)MnH.¹⁹

CONCLUSION

We have described the synthesis, electronic structure, and hydrosilylation activity of the (PDI)Mn dimer, [(Ph₂PEtPDI)Mn]₂. Although the ethylene-bridged substituents of Ph₂PEtPDI have proven too rigid to allow for κ^5 -PDI coordination to Mn following (Ph₂PEtPDI)MnCl₂ reduction, dimerization via η^2 -imine coordination occurs to fill the coordination sphere of Mn and stabilize formally zero-valent [(Ph₂PEtPDI)Mn]₂. Dimer formation was not found to prevent carbonyl hydrosilylation or carboxylate dihydrosilylation and competitive turnover frequencies were noted for each transformation. However, it should be noted that slower aldehyde reduction in the presence of pyridine or olefin functionalities was observed along with delayed onset relative to propylene-bridged (Ph₂PPrPDI)Mn. On the basis of experimental observations and our inability to observe a Ph₂PEtPDI-supported Mn hydride complex, it is proposed that [(Ph₂PEtPDI)Mn]₂ dissociates into monomeric units that mediate carbonyl and carboxylate hydrosilylation through a modified Ojima mechanism.

EXPERIMENTAL SECTION

General Considerations. Unless otherwise stated, all synthetic reactions were performed in an MBraun glovebox under an atmosphere of purified nitrogen. Aldrich anhydrous solvents were purified using a Pure Process Technology solvent system and stored in the glovebox over activated 4 Å molecular sieves and potassium (purchased from Sigma-Aldrich) before use. Benzene-*d*₆ was purchased from Cambridge Isotope Laboratories and dried over 4 Å molecular sieves before use. 1,3,5,7-Cyclooctatetraene and 2-(diphenylphosphino)ethylamine were purchased from Strem Chemicals Inc. and used as received. Manganese powder, metallic mercury, (THF)₂MnCl₂, 4-fluorobenzaldehyde, and Celite were purchased from Acros. 2-Naphthaldehyde, 4-bromobenzaldehyde, 4-chlorobenzaldehyde, pyridine-3-carboxaldehyde, 3-cyclohexene-1-carboxaldehyde, acetophenone, and *p*-toluenesulfonic acid monohydrate were received from TCI America. Methyl formate, ethyl formate, anisyl formate, octyl formate, benzyl formate, and isoamyl formate were also purchased from TCI America. PhSiH₃ and 4-cyanobenzaldehyde were obtained from Oakwood Products. Ethyl acetate was obtained from Alfa Aesar. All the liquid substrates were scrupulously dried over 4 Å molecular sieves or distilled if necessary before use. The solid substrates were recrystallized from diethyl ether or tetrahydrofuran before use. Ph₂PEtPDI was prepared according to literature procedure.²¹

Solution ¹H and ¹³C nuclear magnetic resonance (NMR) spectra were recorded in benzene-*d*₆ at room temperature on a Varian 400-MR NMR spectrometer. All ¹H and ¹³C NMR chemical shifts (ppm) are reported relative to Si(CH₃)₄ using ¹H (residual) and ¹³C chemical

shifts of the solvent as secondary standards. ^{31}P NMR shifts are referenced relative to H_3PO_4 as an external standard. Elemental analysis was conducted at Robertson Microlit Laboratories Inc. (Ledge wood, NJ). Although the results lie slightly outside the range viewed as establishing analytical purity, they are provided to illustrate the best values obtained to date. Solid-state magnetic susceptibility was recorded at 25 °C using a Johnson Matthey magnetic susceptibility balance calibrated with $\text{HgCo}(\text{SCN})_4$. Solution state magnetic susceptibility was determined via Evans method on the Varian 400 MHz NMR spectrometer. Melting point determinations were performed using a DigiMelt apparatus.

X-ray Crystallography. Single crystals suitable for X-ray diffraction were coated with polyisobutylene oil in the glovebox and transferred to a glass fiber with Apiezon N grease, which was then mounted on the goniometer head of a Bruker APEX Diffractometer equipped with Mo $K\alpha$ radiation. A hemisphere routine was used for data collection and determination of the lattice constants. The space group was identified and the data was processed using the Bruker SAINT+ program and corrected for absorption using SADABS. The structure was solved using direct methods (SHELXS) completed by subsequent Fourier synthesis and refined by full-matrix, least-squares procedures on $[F^2]$. Crystallographic parameters for complex **2** are provided in Table S1.

Electron Paramagnetic Resonance Spectroscopy. Instrumentation. Studies were performed at the EPR Facility of Arizona State University. Continuous wave (CW) EPR spectra were recorded at 107 K using a Bruker ELEXSYS E580 CW X-band spectrometer (Bruker, Rheinstetten, Germany) equipped with a liquid nitrogen temperature control system (ER 4131VT). The magnetic field modulation frequency was 100 kHz with a field modulation of 1 mT peak-to-peak. The microwave power was 4 mW, the microwave frequency was 9.40 GHz, and the sweep time was 84 s.

Spin Hamiltonian. The EPR spectrum of $[(\text{Ph}_2\text{PEt})\text{PDI}]\text{Mn}_2$ was analyzed considering that this manganese complex contains two identical molecules. Each of these molecules was assumed to carry one net unpaired electron (see Results section), thereby yielding a triplet state ($S = 1$) for the manganese complex. Consequently, the EPR data was fit using a spin Hamiltonian, H , containing the electron Zeeman interaction with the applied magnetic field B_0 , the zero-field interaction, and the hyperfine coupling (hfc) interactions with two equivalent ^{55}Mn ($I = 5/2$):²⁵

$$H = \beta_e S \cdot g \cdot B_0 + h S \cdot D \cdot S + \sum_{i=1}^2 h S \cdot A^{Mn_i} \cdot I^{Mn_i} \quad (1)$$

where S is the electron spin operator, I^{Mn_i} are the nuclear spin operators of the two equivalent ^{55}Mn , D and A^{Mn_i} are the zero-field interaction and hfc tensors, respectively, all in frequency units, g is the electronic g -tensor, β_e is the electron magneton, and h is Planck's constant. The so-called zero-field interaction occurs in the absence of an applied magnetic field because of electron–electron repulsion. For a triplet state ($S = 1$) system, the zero-field interaction partially breaks the degeneracy of the triplet causing the energy of the levels, corresponding to $m_S = \pm 1$, to shift by the term Dm_S^2 , where D is the axial zero-field splitting (ZFS) parameter and m_S is the magnetic quantum number of the triplet ($0, \pm 1$). Additional shifting of the energy of the $m_S = \pm 1$ doublet is induced by the rhombic zero-field splitting term, which is characterized by the parameter E . The electron Zeeman interaction contributes to the Hamiltonian when an external magnetic field is applied. This interaction is anisotropic and depends on the relative orientation between the magnetic field and the molecular axes of the manganese complex. The Zeeman interaction breaks the remaining degeneracy of the $m_S = \pm 1$ doublet causing an additional shift given by the term $g\beta_e B_0 m_S / h$ in the energy of these levels, where g is the g -value. A further energetic consideration is the contribution of the hfc interactions, which represents the interaction between the magnetic moment of the unpaired electron system and the magnetic moments of two equivalent ^{55}Mn nuclei. The hyperfine interaction is described as first-order by the expression $A^{Mn_i} m_S (m_{11} + m_{12})$, where A^{Mn_i} is the hfc interaction along an arbitrary magnetic field

direction and m_{11} and m_{12} are the magnetic quantum numbers of the ^{55}Mn nuclei.

Fitting of EPR Spectra. To quantitatively compare experimental and simulated spectra, we divided the spectra into N intervals, i.e., we treated the spectrum as an N -dimensional vector R . Each component R_j has the amplitude of the EPR signal at a magnetic field B_j , with j varying from 1 to N . The amplitudes of the experimental and simulated spectra were normalized so that the span between the maximum and minimum values of R_j is 1. We compared the calculated amplitudes R_j^{calc} of the signal with the observed values R_j defining a root-mean-square deviation σ by

$$\sigma(p_1, p_2, \dots, p_n) = \left[\sum_j (R_j^{\text{calc}}(p_1, p_2, \dots, p_n) - R_j^{\text{exp}})^2 / N \right]^{1/2} \quad (2)$$

where the sums are over the N values of j , and p 's are the fitting parameters that produced the calculated spectrum. For our simulations, N was set equal to 1024. The EPR spectra were simulated using EasySpin (v 5.1.10), a computational package developed by Stoll and Schweiger²⁶ and based on Matlab (The MathWorks, Natick, MA). EasySpin calculates EPR resonance fields using the energies of the states of the spin system obtained by direct diagonalization of the spin Hamiltonian (see eq 1). The EPR fitting procedure used a Monte Carlo type iteration to minimize the root-mean-square deviation, σ (see eq 2) between measured and simulated spectra. We searched for the optimum values of the following parameters: the principal components of g (i.e., g_x, g_y , and g_z), the ZFS parameters, D and E , the principal components of the hfc tensor A^{Mn_i} (i.e., $A_x^{Mn_i}, A_y^{Mn_i}$, and $A_z^{Mn_i}$) and the peak-to-peak line-widths ($\Delta B_x, \Delta B_y$, and ΔB_z).

Preparation of $(\text{Ph}_2\text{PEt})\text{PDI}]\text{MnCl}_2$ (1). A thick-walled glass tube was charged with 0.269 g of Ph_2PEtPDI (0.461 mmol) and 0.124 g of $(\text{THF})_2\text{MnCl}_2$ (0.461 mmol) in approximately 20 mL of toluene. The tube was sealed under nitrogen atmosphere and heated at 125 °C for 120 h. The resulting pale orange slurry was vacuum filtered, and the solid was washed with toluene (4×5 mL) and diethyl ether (3×5 mL) to remove any excess ligand. Finally, drying yielded 0.307 g (94%) of a pale orange solid identified as **1**. Elemental analysis for $\text{C}_{37}\text{H}_{37}\text{N}_3\text{P}_2\text{MnCl}_2$: calcd. C, 62.45%; H, 5.24%; N, 5.90%; Found C, 61.81%; H, 5.10%; N, 5.72%. Magnetic moment (Gouy balance, 25 °C): 6.0 μ_B . ^1H NMR (CDCl_3 , 25 °C): No resonances observed. ^{13}C NMR (CDCl_3 , 25 °C): No resonances observed.

Preparation of $[(\text{Ph}_2\text{PEt})\text{PDI}]\text{Mn}_2$ (2). A 20 mL scintillation vial was charged with 4.716 g (23.58 mmol) of Hg^0 in 5 mL of THF and 0.027 g (1.18 mmol) of freshly cut Na^0 was added. The amalgam was stirred for 25 min while it became clear. Then, 13.3 μL (0.118 mmol) of 1,3,5,7-cyclooctatetraene was added and stirred for 5 min while it turned pale yellow. A 10 mL THF slurry of **1** (0.168 g, 0.236 mmol) was then added and an instantaneous color change to red was noticed. The mixture was stirred at room temperature for 6 h. The red solution was filtered through Celite and THF was removed *in vacuo*. The resulting red film was washed with pentane (2×5 mL) and dried again. It was then dissolved in 10 mL of toluene and filtered through a Celite column. After concentrating the filtrate and layering with diethyl ether, recrystallization at -35 °C yielded 0.113 g (38%) of red crystals identified as **2** upon drying. Elemental analysis for $\text{C}_{74}\text{H}_{74}\text{N}_6\text{P}_4\text{Mn}_2$: Calcd. C, 69.37%; H, 5.82%; N, 6.56%. Found C, 69.36%; H, 6.35%; N, 6.21%. Magnetic moment (Evans method, 25 °C): $\mu_{\text{eff}} = 3.3 \mu_B$. ^1H NMR (benzene- d_6 , 23 °C): 32.26 (peak width at half height = 514 Hz), 26.23 (153 Hz). ^{13}C NMR (benzene- d_6 , 25 °C): No resonances observed. $\{^1\text{H}\}^{31}\text{P}$ NMR (benzene- d_6 , 25 °C): -58.49 (487 Hz).

General Method of Aldehyde Hydrosilylation Using 0.05 mol % **2 (0.1 mol % Relative to Mn).** In the glovebox, a 20 mL scintillation vial was charged with 0.0022 g of **2** (0.0017 mmol). To the catalyst, an equimolar mixture of PhSiH_3 (3.40 mmol) and aldehyde (3.40 mmol) was added. **CAUTION: This reaction is exothermic and vigorous bubbling occurs, which we believe is due to reactant vaporization.** After 2 min, the reaction was exposed to oxygen to deactivate the catalyst. The resulting colorless solution was filtered through Celite and analyzed by ^1H NMR spectroscopy to determine percent conversion. The fractions were recombined and hydrolyzed

with 2 mL of 10% aqueous NaOH solution upon stirring for 2 h at room temperature. The organic layer was extracted with diethyl ether (3 × 4 mL) and dried over anhydrous Na₂SO₄. The solvent was removed *in vacuo* at 40 °C to yield the corresponding alcohol.

General Method of Aldehyde Hydrosilylation Using 0.005 mol % 2 (0.01 mol % Relative to Mn). In the glovebox, a 100 mL round-bottom flask was charged with 0.0014 g of 2 (0.0011 mmol). To the catalyst, an equimolar mixture of PhSiH₃ (22.6 mmol) and aldehyde (22.6 mmol) was added. **CAUTION: This reaction is exothermic and vigorous bubbling occurs, which we believe is due to reactant vaporization.** After 2 min, the reaction was exposed to oxygen to deactivate the catalyst. The colorless solution obtained was filtered through Celite and analyzed by ¹H NMR spectroscopy to determine the percent conversion. The fractions were recombined and hydrolyzed with 2 mL of 10% aqueous NaOH solution upon stirring for 2 h at room temperature. The organic layer was extracted with diethyl ether (3 × 4 mL) and dried over anhydrous Na₂SO₄. The solvent was removed *in vacuo* at 40 °C to yield the corresponding alcohol.

General Method of Formate Dihydrosilylation Using 0.01 mol % 2 (0.02 mol % Relative to Mn). In the glovebox, a 100 mL round-bottom flask was charged with 0.002 g of 2 (0.002 mmol). To the catalyst, an equimolar mixture of PhSiH₃ (20.0 mmol) and formate (20.0 mmol) was added. **CAUTION: This reaction is exothermic and vigorous bubbling occurs, which we believe is due to reactant vaporization.** After 30 min, the reaction was exposed to oxygen to deactivate the catalyst. The colorless solution obtained was filtered through Celite and analyzed by ¹H NMR spectroscopy to determine the percent conversion. The fractions were recombined and hydrolyzed with 2 mL of 10% aqueous NaOH solution upon stirring for 2 h at room temperature. The organic layer was extracted with diethyl ether (3 × 4 mL) and dried over anhydrous Na₂SO₄. The solvent was removed *in vacuo* at 40 °C to yield the corresponding alcohol.

■ ASSOCIATED CONTENT

Supporting Information

The Supporting Information is available free of charge on the ACS Publications website at DOI: 10.1021/acs.organomet.7b00423.

Compound characterization, metrical parameters for 2 and detailed hydrosilylation procedures (PDF)

Accession Codes

CCDC 1552985 contains the supplementary crystallographic data for this paper. These data can be obtained free of charge via www.ccdc.cam.ac.uk/data_request/cif, or by emailing data_request@ccdc.cam.ac.uk, or by contacting The Cambridge Crystallographic Data Centre, 12 Union Road, Cambridge CB2 1EZ, UK; fax: +44 1223 336033.

■ AUTHOR INFORMATION

Corresponding Author

*E-mail: ryan.trovitch@asu.edu.

ORCID

Ryan J. Trovitch: 0000-0003-4935-6780

Notes

The authors declare no competing financial interest.

■ ACKNOWLEDGMENTS

This material is based upon work supported by the National Science Foundation under Grant No. 1651686. Acknowledgement is also made to the Donors of the American Chemical Society Petroleum Research Fund for support of this research. We acknowledge Dr. Brian R. Cherry for NMR assistance.

■ REFERENCES

- (1) Hudlický, M. *Reductions in Organic Chemistry*, 2nd ed.; American Chemical Society: Washington, DC, 1996.
- (2) (a) Seyden-Penne, J. *Reductions by the Alumino- and Borohydrides in Organic Synthesis*, 2nd ed.; Wiley-VCH: New York, 1997. (b) Abdel-Magid, A. F. *Reductions in Organic Synthesis*; American Chemical Society: Washington, DC, 1996.
- (3) Rylander, P. N. *Catalytic Hydrogenation in Organic Syntheses*; Academic Press: New York, NY, 1979.
- (4) Ojima, I. *Chem. Org. Silicon Compd.* **1989**, 2, 1479–1526.
- (5) For an influential example, see Ojima, I.; Kogure, T. *Organometallics* **1982**, 1, 1390–1399.
- (6) (a) Collman, J. P.; Hegedus, L. S.; Norton, J. R.; Finke, R. G. *Principles and Applications of Organotransition Metal Chemistry*; University Science Books: Sausalito, CA, 1987. (b) Hartwig, J. F. *Organotransition Metal Chemistry – From Bonding to Catalysis*; University Science Books: Sausalito, CA, 2010.
- (7) Leading Fe carbonyl hydrosilylation catalysts according to TOF: (a) Yang, J.; Tilley, T. D. *Angew. Chem., Int. Ed.* **2010**, 49, 10186–10188. (b) Ruddy, A. J.; Kelly, C. M.; Crawford, S. M.; Wheaton, C. A.; Sydora, O. L.; Small, B. L.; Stradiotto, M.; Turculet, L. *Organometallics* **2013**, 32, 5581–5588.
- (8) Leading Co carbonyl hydrosilylation catalysts according to TOF: (a) Niu, Q.; Sun, H.; Li, X.; Klein, H.-F.; Flörke, U. *Organometallics* **2013**, 32, 5235–5238. (b) Nesbit, M. A.; Suess, D. L. M.; Peters, J. C. *Organometallics* **2015**, 34, 4741–4752.
- (9) Leading Ni carbonyl hydrosilylation catalysts according to TOF: (a) Postigo, L.; Royo, B. *Adv. Synth. Catal.* **2012**, 354, 2613–2618. (b) Bheeter, L. P.; Henrion, M.; Brelot, L.; Darcel, C.; Chetcuti, M. J.; Sortais, J.-B.; Ritleng, V. *Adv. Synth. Catal.* **2012**, 354, 2619–2624.
- (10) Leading Cu carbonyl hydrosilylation catalysts according to TOF: (a) Lipshutz, B. H.; Noson, K.; Chrisman, W.; Lower, A. *J. Am. Chem. Soc.* **2003**, 125, 8779–8789. (b) Wu, J.; Ji, J.-X.; Chan, A. S. C. *Proc. Natl. Acad. Sci. U. S. A.* **2005**, 102, 3570–3575.
- (11) Leading Zn carbonyl hydrosilylation catalysts according to TOF: (a) Rit, A.; Zanardi, A.; Spaniol, T. P.; Maron, L.; Okuda, J. *Angew. Chem., Int. Ed.* **2014**, 53, 13273–13277. (b) Sattler, W.; Ruccolo, S.; Chaijan, M. R.; Allah, T. N.; Parkin, G. *Organometallics* **2015**, 34, 4717–4731.
- (12) (a) Trovitch, R. J. *Synlett* **2014**, 25, 1638–1642. (b) Valyaev, D. A.; Lavigne, G.; Lugan, N. *Coord. Chem. Rev.* **2016**, 308, 191–235.
- (13) Manganese carbonyl reduction catalysts that utilize H₂ or boranes have recently been described. See (a) Zhang, G.; Zeng, H.; Wu, J.; Yin, Z.; Zheng, S.; Fettingner, J. C. *Angew. Chem., Int. Ed.* **2016**, 55, 14369–14372. (b) Elangovan, S.; Topf, C.; Fischer, S.; Jiao, H.; Spannenberg, A.; Baumann, W.; Ludwig, R.; Junge, K.; Beller, M. *J. Am. Chem. Soc.* **2016**, 138, 8809–8814. (c) Kallmeier, F.; Irrgang, T.; Dietel, T.; Kempe, R. *Angew. Chem., Int. Ed.* **2016**, 55, 11806–11809. (d) Zirakzadeh, A.; de Aguiar, S. R. M. M.; Stöger, B.; Widhalm, M.; Kirchner, K. *ChemCatChem* **2017**, 9, 1744–1748. (e) Widegren, M. B.; Harkness, G. J.; Slawin, A. M. Z.; Cordes, D. B.; Clarke, M. L. *Angew. Chem., Int. Ed.* **2017**, 56, 5825–5828. (f) Vasilenko, V.; Blasius, C. K.; Wadepohl, H.; Gade, L. H. *Angew. Chem., Int. Ed.* **2017**, 56, 8393–8397.
- (14) Cavanaugh, M. B.; Gregg, B. T.; Cutler, A. R. *Organometallics* **1996**, 15, 2764–2769.
- (15) This paper describes the conversion of esters into ethers via deoxygenation as opposed to ester dihydrosilylation to yield a mixture of silyl ethers. Mao, Z.; Gregg, B. T.; Cutler, A. R. *J. Am. Chem. Soc.* **1995**, 117, 10139–10140.
- (16) (a) Son, S. U.; Paik, S.-J.; Lee, I. S.; Lee, Y.-A.; Chung, Y. K.; Seok, W. K.; Lee, H. N. *Organometallics* **1999**, 18, 4114–4118. (b) Son, S. U.; Paik, S.-J.; Chung, Y. K. *J. Mol. Catal. A: Chem.* **2000**, 151, 87–90. (c) Zheng, J.; Chevance, S.; Darcel, C.; Sortais, J.-B. *Chem. Commun.* **2013**, 49, 10010–10012. (d) Zheng, J.; Elangovan, S.; Valyaev, D. A.; Brousses, R.; César, V.; Sortais, J.-B.; Darcel, C.; Lugan, N.; Lavigne, G. *Adv. Synth. Catal.* **2014**, 356, 1093–1097. (e) Valyaev, D. A.; Wei, D.; Elangovan, S.; Cavailles, M.; Dorcet, V.; Sortais, J.-B.; Darcel, C.; Lugan, N. *Organometallics* **2016**, 35, 4090–4098.

- (f) Vijjamarri, S.; Chidara, V. K.; Du, G. *ACS Omega* **2017**, *2*, 582–591.
- (17) Chidara, V. D.; Du, G. *Organometallics* **2013**, *32*, 5034–5037.
- (18) Mukhopadhyay, T. K.; Flores, M.; Groy, T. L.; Trovitch, R. J. *J. Am. Chem. Soc.* **2014**, *136*, 882–885.
- (19) Mukhopadhyay, T. K.; Rock, C. L.; Ashley, D. C.; Hong, M.; Groy, T. L.; Baik, M.-H.; Trovitch, R. J. *J. Am. Chem. Soc.* **2017**, *139*, 4901–4915.
- (20) Ghosh, C.; Mukhopadhyay, T. K.; Flores, M.; Groy, T. L.; Trovitch, R. J. *Inorg. Chem.* **2015**, *54*, 10398–10406.
- (21) Ben-Daat, H.; Hall, G. B.; Groy, T. L.; Trovitch, R. J. *Eur. J. Inorg. Chem.* **2013**, *2013*, 4430–4442.
- (22) Bart, S. C.; Chlopek, K.; Bill, E.; Bouwkamp, M. W.; Lobkovsky, E.; Neese, F.; Wieghardt, K.; Chirik, P. J. *J. Am. Chem. Soc.* **2006**, *128*, 13901–13912.
- (23) (a) Khusniyarov, M. M.; Harms, K.; Burghaus, O.; Sundermeyer, J. *Eur. J. Inorg. Chem.* **2006**, *2006*, 2985–2996. (b) Muresan, N.; Chlopek, K.; Weyhermüller, T.; Neese, F.; Wieghardt, K. *Inorg. Chem.* **2007**, *46*, 5327–5337.
- (24) The leading TOF for each metal previously reported to mediate carboxylate dihydrosilylation via selective acyl C–O cleavage is provided: (a) For Ti (TOF = 33 h⁻¹): Barr, K. J.; Berk, S. C.; Buchwald, S. L. *J. Org. Chem.* **1994**, *59*, 4323–4326. (b) For V (TOF = 0.8 h⁻¹): Pehlivan, L.; Métay, E.; Laval, S.; Dayoub, W.; Delbrayelle, D.; Mignani, G.; Lemaire, M. *Eur. J. Org. Chem.* **2011**, *2011*, 7400–7406. (c) For Mn, see ref 19. (d) For Fe (TOF as high as 100 h⁻¹), see ref 7b. (e) For Zn (TOF = 12.5 h⁻¹): Mimoun, H. *J. Org. Chem.* **1999**, *64*, 2582–2589. (f) For Mo (TOF = 1.0 h⁻¹): Fernandes, A. C.; Romão, C. C. *J. Mol. Catal. A: Chem.* **2006**, *253*, 96–98. (g) For Ru (TOF = 33 h⁻¹, based on Ru): Matsubara, K.; Iura, T.; Maki, T.; Nagashima, H. *J. Org. Chem.* **2002**, *67*, 4985–4988. (h) For Rh (TOF = 16.7 h⁻¹): Ohta, T.; Kamiya, M.; Kusui, K.; Michibata, T.; Nobutomo, M.; Furukawa, I. *Tetrahedron Lett.* **1999**, *40*, 6963–6966. (i) For Pd (TOF = 2.8 h⁻¹): Nakanishi, J.; Tatamidani, H.; Fukumoto, Y.; Chatani, N. *Synlett* **2006**, *2006*, 869–872.
- (25) Weil, J. A.; Bolton, J. R. *Electron paramagnetic resonance: Elementary theory and practical applications*; Wiley: Hoboken, NJ, 2007.
- (26) Stoll, S.; Schweiger, A. *J. Magn. Reson.* **2006**, *178*, 42–55.